Enabling Uniform and Accurate Control of Cycling Pressure for All-Solid-State Batteries

Yu-Ting Chen[1†], Jihyun Jang[2,3†], Jin An Sam Oh[2], So-Yeon Ham[1], Hedi Yang[4], Dong-Ju Lee[2], Marta Vicencio[2], Jeong Beom Lee[5], Darren H. S. Tan[2], Mehdi Chouchane[4], Ashley Cronk[1], Min-Sang Song[5], Yijie Yin[1], Jianting Qian[1], Zheng Chen[1,2,6,7]*, and Ying Shirley Meng[1,2,4,6]*

[1] Program of Materials Science and Engineering, University of California San Diego, La Jolla, California 92093, United States

[2] Department of NanoEngineering, University of California San Diego, La Jolla, California 92093, United States of America

[3] Department of Chemistry, Sogang University, 35 Baekbeom-ro, Mapo-Gu, Seoul 04107, Korea

[4] Pritzker School of Molecular Engineering, The University of Chicago, Chicago, IL 60637, United States

[5] LG Energy Solution, Ltd., LG Science Park, Magokjungang 10-ro, Gangseo-gu, Seoul 07796, Korea.

[6] Sustainable Power & Energy Center (SPEC), University of California San Diego, La Jolla, California 92093, United States

[7] Program of Chemical Engineering, University of California San Diego, La Jolla, California 92093, United States

*zhc199@ucsd.edu, shmeng@uchicago.edu

[†]Yu-Ting Chen and Jihyun Jang contributed equally to this work.

Keywords: All-solid-state batteries, pouch cells, isostatic cycling pressure

Abstract

All-solid-state batteries are emerging as potential successors in energy storage technologies due to their increased safety, stemming from replacing organic liquid electrolytes in conventional Li-ion batteries with less flammable solid-state electrolytes. However, All-solid-state batteries require precise control over cycling pressure to maintain effective interfacial contacts between materials. Traditional uniaxial cell holders, often used in battery research, face challenges in accommodating electrode volume changes, providing uniform pressure distribution, and maintaining consistent pressure over time. This study introduces isostatic pouch cell holders utilizing air as pressurizing media to achieve uniform and accurately regulated cycling pressure. $LiNi_{0.8}Co_{0.1}Mn_{0.1}O_2$ | Li_6PS_5Cl | Si pouch cells were fabricated and tested under 1 to 5 MPa pressures, revealing improved electrochemical performance with higher cycling pressures, with 2 MPa as the minimum for optimal operation. A bilayer pouch cell with a theoretical capacity of 100 mAh, cycled with an isostatic pouch cell holder, demonstrated a first-cycle Coulombic efficiency of 76.9% and a discharge capacity of 173.6 mAh g^{-1} (88.1 mAh), maintaining 83.6% capacity after 100 cycles. These findings underscore the effectiveness of isostatic pouch cell holders in enhancing the performance and practical application of All-solid-state batteries.

Table of Contents

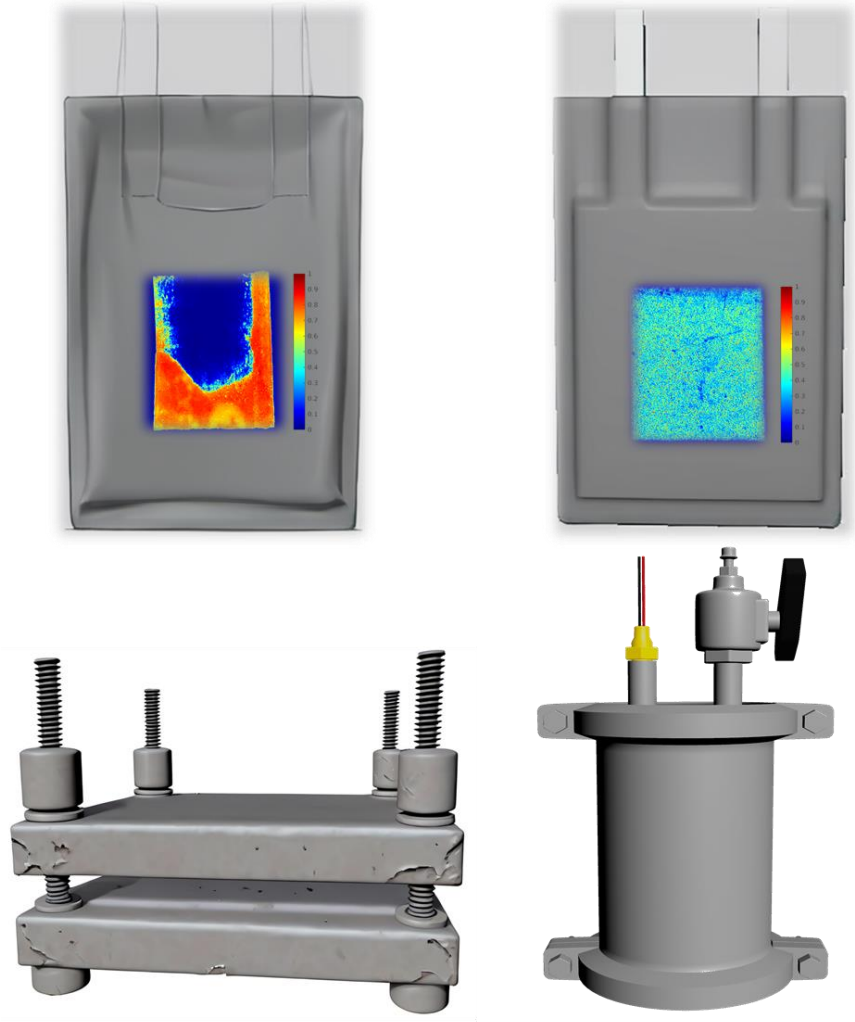

Main Text

All-solid-state batteries (ASSBs) are hailed as one of the next generation energy storage technologies and tremendous efforts have been invested to their development. As solid-state electrolytes (SSEs) are employed to replace liquid electrolytes in conventional Li batteries, ASSBs exhibit reduced flammability and leakage issues.[1-4] Moreover, anodes with high specific capacity, such as pure Si,[5-6] have been reported to achieve long cycle life in ASSBs, but meets challenges in liquid electrolytes as Si will suffer from pulverization during cycling resulting in continuous solid electrolyte interphase (SEI) formation.[7-11] Despite these advantages, there are many engineering challenges for ASSBs stemming from solid-solid interfacial contacts.[12] The inability to flow and infiltrate into voids in the electrode is a double edge sword: it limits the SEI formation, but volumetric changes in the electrode can potentially cause detachment of electrode material – SSE interfaces.[13-14] This leads to deteriorating electrochemical reaction in the ASSBs. As such, pressure becomes a crucial factor to maintain intimate interfacial contact and ensure the performance of ASSBs – not only in cell fabrication, but also during cell cycling.

Pellet-type ASSBs are usually employed in research labs for electrochemical tests. A polymer die and a pair of metal plungers are employed to contain and apply fabrication pressure to pelletize the materials. During electrochemical tests, a cell holder consisting of bolts, nuts and plates is required to apply cycling pressure and the metal plungers serve as current collectors (**Figure 1a**). As most inorganic SSEs are brittle, SSE layers typically have a high thickness of approximately 500 μm to guarantee a sufficient strength to support the cells mechanically. This reduces the energy density of ASSBs, as SSE layers do not store energy.[15-18] Moreover, due to the friction at the die walls during uniaxial compaction and parallelism tolerance at the metal plungers, it is challenging to achieve a uniform density distribution throughout the whole pellet, and this may negatively affect its electrochemical performance.[19] By having thinner layer thickness, larger electrode area, and no requirement of polymer dies, pouch cells not only exhibit significantly higher energy density, but also achieve better density distribution after calendering (**Figure 1b**). As the wrapping materials of pouch cells are flexible, isostatic pressure can be applied to further improve the density uniformity, which has been well-demonstrated in the literature.[19-20]

Although multiple groups have claimed to demonstrate solid-state pouch cells in the literature, many adulterate excess amount of polymer binders, Li salts, and even solvents to boost the performance. These defeat the safety feature of ASSBs. Several all-solid-state pouch cells (ASSPC) with more than 3 mAh cm^{-2} employing only inorganic SSE (with low amounts of binders) were reported (**Table 1**), which is similar to or higher than that in commercial Li batteries. Nevertheless, many cells were tested at C-rates lower than 0.1 C, and elevated temperature was required to realize higher C-rates and areal capacities. As SSEs do not flow and conform to the shape of electrode materials like liquid electrolytes, a pressure must be applied to ASSBs to ensure intimate interfacial contact, both in fabrication and during cycling.[12, 19, 21] Most articles report only fabrication pressure, typically 300 to 500 MPa, without mentioning cycling pressure. However, cycling pressure is a more important metric for commercialization, as high cycling pressure will vastly increase the dead weight of the system and sacrifice the module energy density. Since a low cycling pressure usually results in insufficient interfacial contact, and thus worse electrochemical performance of ASSBs, it is critical to design cell holders that provide uniform cycling pressure.

Pouch cell holders consisting of bolts, nuts, and rigid plates are employed in most articles to apply uniaxial pressure to pouch cells (**Figure 1c**). Some may attach bearings between moving plates and bolts to ensure smooth movement and parallelism. However, several studies have observed that the cycling pressure of ASSBs changes during cell cycling due to the volume change of electrode materials.[22-23] For example, Si undergoes 300% of volume expansion and the thickness of Li metal anodes increases approximately 5 μm when each mAh cm^{-2} is plated.[24] This may negatively affect their electrochemical performance, especially when pressure sensitive materials, such as Li metal, are used. To address this problem, Ham et al incorporated springs into the cell holders to accommodate cycling volume change. Such a design successfully reduced the cycling pressure change of a $LiNi_{0.8}Co_{0.1}Mn_{0.1}O_2$ (NCM811) | Li cell from 2 MPa to less than 0.5 MPa, and thus doubled its critical current density at 40°C.[23] Inspired by this work, an improved uniaxial pouch cell holder (UPCH) design containing springs and rubber gaskets was also proposed (**Figure 1d**).[16] Nevertheless, rubber and springs may be susceptible to material fatigue and the applied force would decrease over time. It is noteworthy that the cell pressure may also change if the ambient temperature fluctuates, since the thermal expansion coefficients of pouch cells and bolts are different. As such, pressure regulation systems are required to ensure the stability of cell cycling. Unfortunately, regulating the pressure accurately by turning the bolts is challenging, as the motors need to overcome large friction under high pressure load, and extra effort is needed to synchronize the torque of the bolts in the cell holder. To tackle this issue, fluids, including gases and liquids, can potentially be utilized as pressurizing media to apply isostatic cycling pressure. Gases can be used when light weight, low cost, or low X-ray absorption (e.g., in-situ cell characterization applications) are needed, and liquids can be employed when pressure load and heat dissipation are demanding. Instead of bolts and nuts, an isostatic pouch cell holder (IPCH) requires a chamber and gaskets to contain the pressurized fluid and ASSPCs. A valve is installed to fill or evacuate the fluid, and a wire fit-through is implemented to electrically connect ASSPCs inside the chamber (**Figure 1e**). As fluids are significantly more compressible and conforming than solids, IPCHs can easily accommodate cell volume changes during cycling. Moreover, the pressure regulating systems of pressurized fluids and gases are mature and widely available, and thus maintaining a constant cycling pressure in IPCHs for an extended period of time can be easily achieved, even in an environment with large temperature fluctuation. To verify our perspective, three cell holders, including a bare UPCH with rigid metal surfaces, an improved UPCH with rubber gaskets and springs, and IPCHs were assembled. The electrochemical performances were all tested with ASSPCs at 30°C under cycling pressures from 5 to 1 MPa throughout the whole study. Compared to the past works, which still relied heavily on pellet type ASSBs under high cycling pressures for electrochemical tests, the new concept discussed in this study successfully reduced the demand for cycling pressure and temperature, while increased the energy density and maintained the electrochemical performance of ASSBs, pathing a way towards practical deployment of ASSBs.

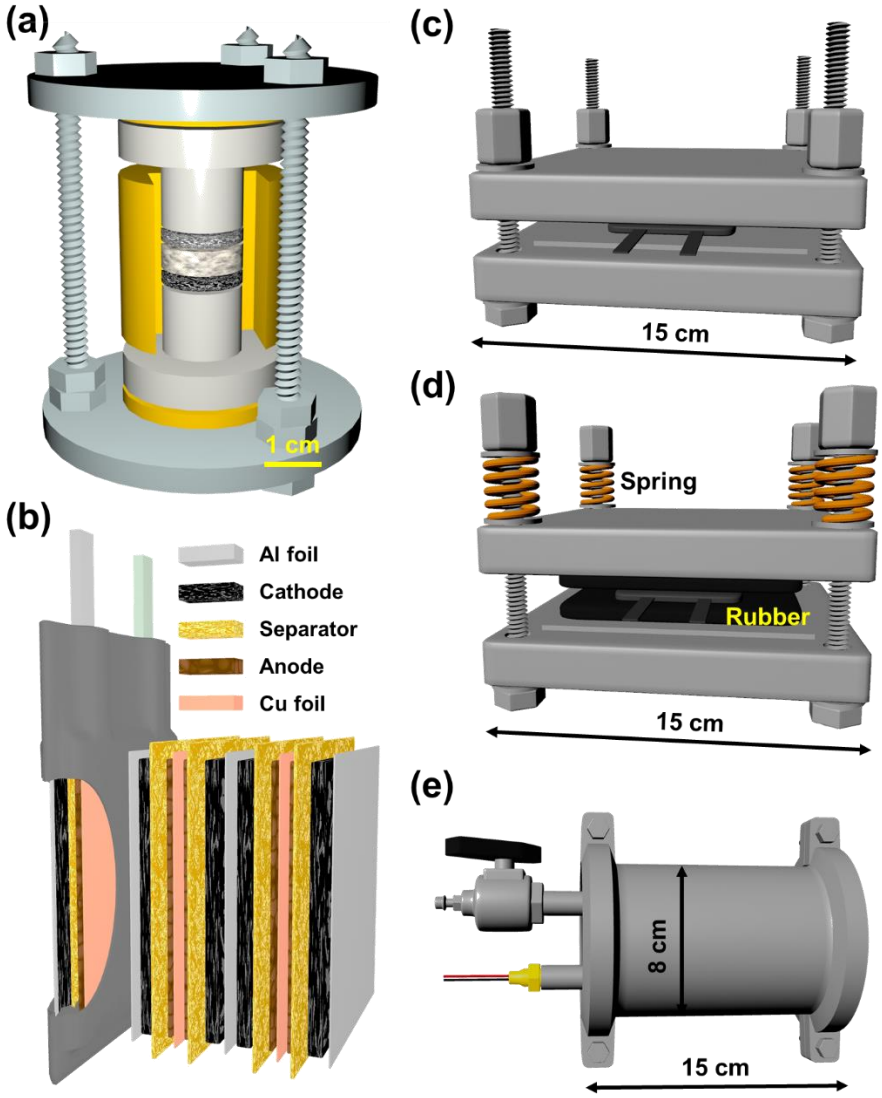

Figure 1. The structure of (a) a plunger cell clamped in a cell holder, and (b) a multilayer pouch cell. The schematic of (c) a bare UPCH with simple metal plates, (d) an improved UPCH with springs and rubber gaskets, and (e) an IPCH.

Table 1. The formats and the cycling conditions of ASSPC reported in the literature.

Ref	Cathode | SSE | Anode	Temperature (°C)	Fabrication pressure (MPa)	Cycling Pressure (MPa)	cycle number	areal capacity (mAh cm^{-2})	C rate	Dimension (cm^2)
[25]	$LiNi_{0.8}Co_{0.15}Al_{0.05}O_2$ | $Li_2SeP_2S_5$ | Graphite	25			100	4.2	0.1 C	8.8x5.3
[26]	$LiNi_{1/3}Co_{1/3}Mn_{1/3}O_2$ | 75 Li_2S·25 P_2S_5 | Graphite	30	330 MPa		10	1.536	C/24	2x2
[27]	$LiNi_{0.6}Co_{0.2}Mn_{0.2}O_2$ | Li_6PS_5Cl | Graphite	30	492 MPa			4.2	0.025 C	8x6

[20]	$LiNi_{0.8}Co_{0.1}Mn_{0.1}O_2$ | Li_6PS_5Cl | C-Ag	60	490 MPa	2	1000	6.8	0.5 C	11.2x6.7
[5]	$LiNi_{09}Co_{0.05}Mn_{0.05}O_2$ | Li_6PS_5Cl | PVD-Si	25	300 MPa	20	50	3	0.05 C	2.5x2.5
[28]	S | Li_6PS_5Cl | Li	30	300 MPa		10	3	0.01 C	3x3
[17]	$LiNi_{0.8}Co_{0.1}Mn_{0.1}O_2$ | Li_6PS_5Cl | LiIn	25			200		0.15 C	6x6
[29]	Sulfur | Solid electrolyte | LiIn	30	500 MPa		50	3.2	0.05 - 2 C	
[30]	$LiNi_{0.6}Co_{0.2}Mn_{0.2}O_2$ | Li_6PS_5Cl | LiIn				100	4	0.1 C	

Results and Discussion

The digital images of the bare UPCH and improved UPCH with springs and rubber gaskets are presented in **Figure S1**. To observe the pressure distribution at 5 MPa, a pressure paper was placed in each cell holder. Upon receiving a pressure higher than its threshold, the pressure paper would turn red, and their digital images were taken (**Figure S2**). To better visualize the pressure distribution, the digital images were converted to color gradient charts. An inhomogeneous pressure distribution was observed for the uniaxial set-up (**Figure 2a and Figure S2a**). When a rigid surface (such as bare metal) is used to apply a uniaxial pressure, areas that are out of contact (e.g., the edges of ASSPCs or imperfect surface flatness of the metal plates forming concave regions) will experience a lower or no pressure. The pressure will concentrate on the rest of the area, resulting in over-pressurization (**Figure 2b and Figure S2b**). These problems were slightly mitigated with the improved UPCH, as rubber gaskets were able to conform to the shape of the metal plates and the ASSPC. Nevertheless, a uniform pressure distribution was still not observed (**Figure 2c**), as the degree of deformation of the rubber gaskets was lower at the areas with larger gaps, resulting in lower pressures (**Figure 2d**). To further improve the uniformity of the cycling pressure, an IPCH was designed, and its digital image and schematic figure are presented in **Figure S3**. The structure of an IPCH consists of a sealed chamber to confine the pressurized fluid and accommodate the ASSPC, a pressure gauge to monitor the chamber pressure, a wire fit-through to enable cycling of the ASSPC sealed in its chamber, and a ball valve able to connect to an air compressor to pressurize, or depressurize the compressed air. Air was selected as the pressurizing medium in this study because of its availability and low cost. Pressure paper was vacuum sealed into a pouch bag, pressurized with an IPCH and the pressure distribution is presented in **Figure 2e** and **Figure S2c**. A uniform pressure distribution was observed. This can be explained by Pascal's principle, which states that a change in pressure applied at any point in the confined fluid at rest is transmitted undiminished throughout the fluid in all directions (**Figure 2f**).

To understand how pressure uniformity affect electrochemical performance, three NCM811 | Li_6PS_5Cl (LPSCl) | Si ASSPCs with a cathode size of 3.5 × 1.5 cm^2 and an areal capacity of 4 mAh cm^{-2} were assembled, calendered at 500 MPa (this cell format was used for the rest of the article), pressurized with the three pouch

cell holders, and cycled under 5 MPa at ambient temperature. The cycling pressure of the UPCH was estimated by the torque values of bolts and nuts, and that of IPCH was by observing the pressure gauge. **Figure 2g** shows voltage profiles of their first cycle. The cell had a soft short during charging if the uniaxial pressure was applied with rigid metal surfaces (bare UPCH), possibly due to having the worst pressure uniformity causing inhomogeneous Li flux in the system. The ASSPCs cycled with the improved UPCH and the IPCH successfully reached 100 cycles (**Figure 2h**). As IPCH provides better pressure uniformity and is less susceptible to structural fatigue (which may lead to cycling pressure drop over time), it exhibited a capacity retention of 126.8 mAh g^{-1} after 100 cycles, higher than that of the improved UPCH (93.5 mAh g^{-1}).

Other than superior electrochemical performance, IPCHs can possibly provide higher energy density than UPCHs at the module level due to the reduced demand of the structural components. There are two physical limitations that IPCHs can avoid: having limited number of cells in a cell stack (**Figure S4a**) and flexing of the pressurizing plates. When a UPCH is used (**Figure S4b**), pressure is transmitted through other ASSPCs. As such, all ASSPCs, including all layers inside every single pouch, must be perfectly aligned, which becomes more challenging and costly as the number of cells in one stack increases. The plates must also be sufficiently thick to resist bending, which may result in applying higher pressure to the edges and lower pressure to the centers of ASSPCs (**Figure S4c**). As fluid is employed as pressurizing media in an IPCH, pressure is identically applied to all points in all directions. Hence, deformation of the vessel wall and arrangement of ASSPCs will not affect the pressure uniformity. As a result, thinner walls can be used in IPCHs to reduce module weight. The estimated required weights of UPCHs and IPCHs using different metal alloys with a pressure rating from 1 to 10 MPa are presented in **Figure S5**. IPCHs are all hypothetically lighter than UPCHs. The weights of IPCHs can be further reduced if polymers and composite materials (which often exhibit high tensile strength but low Young's modulus) are employed. Implementing ASSPC formats with higher energy density, such as jelly roll and Z-stacking, gives IPCHs a further edge, as there are fewer shape limitations for IPCHs. The details for holder weight estimations are discussed in **Note S1**.

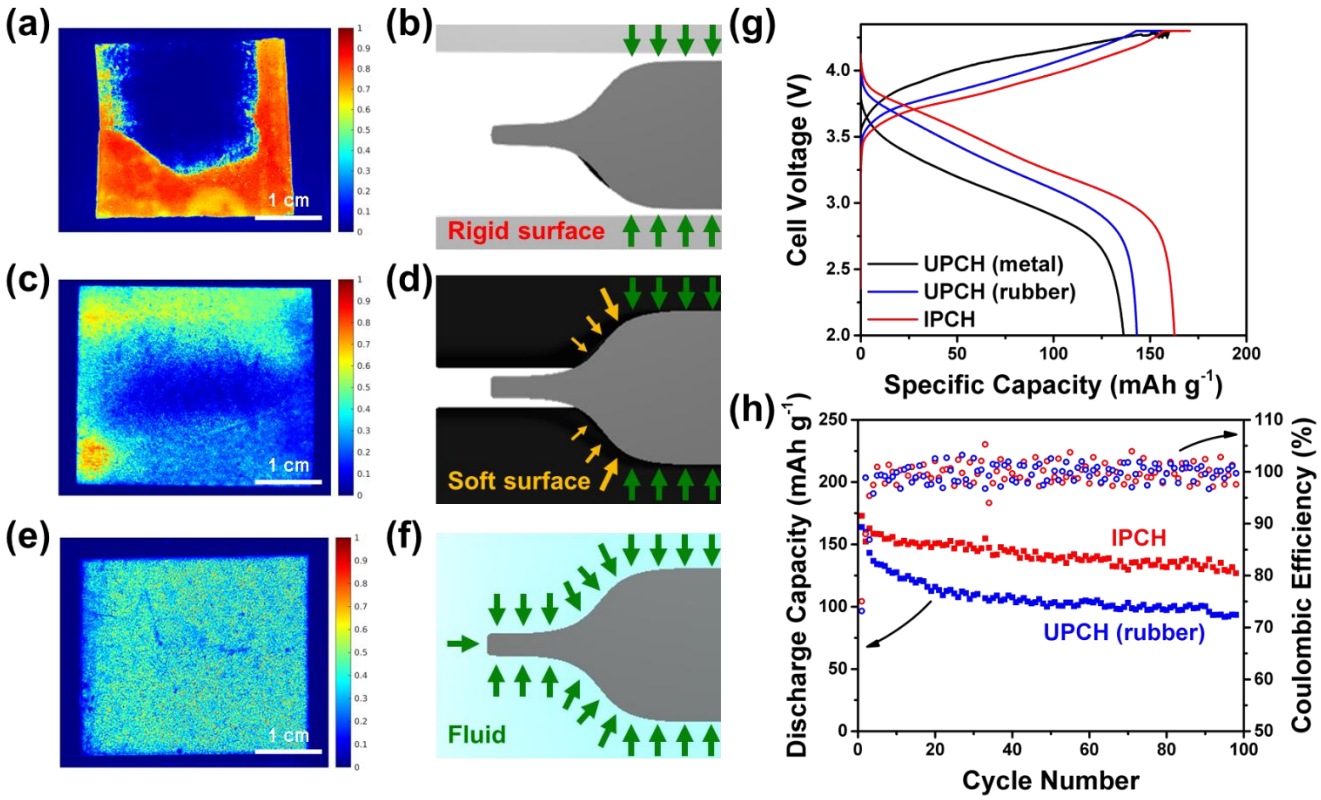

Figure 2. The experimental pressure paper observation and the schematics of the force distribution on the sealing edges of ASSPCs when (a,b) uniaxial pressure is applied by rigid metal surfaces with a bare UPCH, (c,d) uniaxial pressure is applied by soft rubber gaskets with an improved UPCH, and (e,f) isostatic pressure is applied by fluids with an IPCH, respectively. (g) The voltage profiles of first cycle and (h) the reversible discharge capacity of ASSPCs when uniaxial and isostatic pressures were applied.

Taking advantage of accurate pressure control and uniform pressure distribution, the effect of cycling pressure of the IPCHs were further evaluated at 30 °C to avoid the fluctuation of ambient temperature. It is worthy to note that the ASSPCs were activated at 5 MPa, and reduced to the target cycling pressures, ranging from 5 MPa to 1 MPa (**Figure 3a**). At 0.1 C, cells cycled at all pressures except 1 MPa exhibited a similar discharge capacity of approximately 160 mAh g^{-1}, and the slight difference was due to batch variance of cathode composites. A minimum cycling pressure of 2 MPa was required to keep a good interfacial contact in the ASSPCs assembled in this study. The effect of cycling pressure became evident when the C-rate was above 0.3 C. At 1 C, the polarization of the cell grew so drastically that only 30 mAh g^{-1} could be obtained with a cycling pressure of 5 MPa. Nevertheless, ASSPCs cycled above 2 MPa regained most of their discharge capacities when the C-rate decreased back to 0.1 C. Pressures of 5, 3 and 2 MPa, were selected to conduct the long cycling test (**Figure 3b**), and were cycled at a moderate rate of 0.2 C to distinguish the effect of cycling pressure to capacity retention while not vastly deteriorating the discharge capacities according to the rate capability test. As the cycling pressure decreased, it required more cycles for the Coulombic efficiency to reach near 100%, and the initial discharge capacity decreased from 149.7 mAh g^{-1} at 5 MPa to 135.4 mAh g^{-1} at 2 MPa. The capacity retention after 100 cycles also deteriorated from 77.8% at 5 MPa to 47.7% at 2 MPa, due

to loss of interface contact. As electrode materials underwent repetitive volume change, it is crucial to apply pressure to maintain physical contact between SSE and electrode materials, and a higher pressure tends to support intimate interfacial contact. The electrochemical impedance spectroscopy (EIS) of 1st and 100th cycle of the three ASSPCs (**Figure S6, Table S1**) were fitted (**Figure 3c**). Four components were used in the model: the bulk, grain boundary interfaces of SSE, anode, and cathode.[31-33] The interfaces at cathode and anode were combined in the first cycle, as their time constants were highly overlapped and were not able to be deconvoluted. All ASSPCs exhibited very similar SSE impedance values at different cycling pressures and cycle numbers, indicating that SSE separator layers were stable during cycling and not sensitive to cycling pressure. Interestingly, an extra semicircle at lower frequency appeared after 100 cycles. To accurately identify the impedance components, a three-electrode ASSPC, consisting of NCM811 cathode, Si anode and Li metal as the working, counter and reference electrodes, respectively, was assembled and analyzed (**Figure 3d and Figure S7a**).[34] After 10 cycles at 5 MPa, the Nyquist plots (**Figure 3e**) indicated that the cathode contributed much more to the impedance than the anode. Thus, the smaller semicircle was assigned to anode. It is worthy to note that the anode potential in **Figure S7b** is approximately 250 to 500 mV vs Li/Li$^+$, which is the redox potential of Si,[11, 35-38] indicates that the small anode impedance did not originate from short-circuiting between anode and reference electrodes. The success of the three-electrode ASSPC also highlighted the ability of IPCH to apply uniform pressure to uneven surfaces, as the thickness of Li, Si and NCM811 electrodes were not identical. When the cycling pressure decreased from 5 to 3 and 2 MPa, both cathode and anode impedance approximately doubled. This indicates that lower cycling pressures resulted in more loss in the physical contacts and such loss accumulated as it cycles. Consequently, it led to increased polarization and more capacity fading.

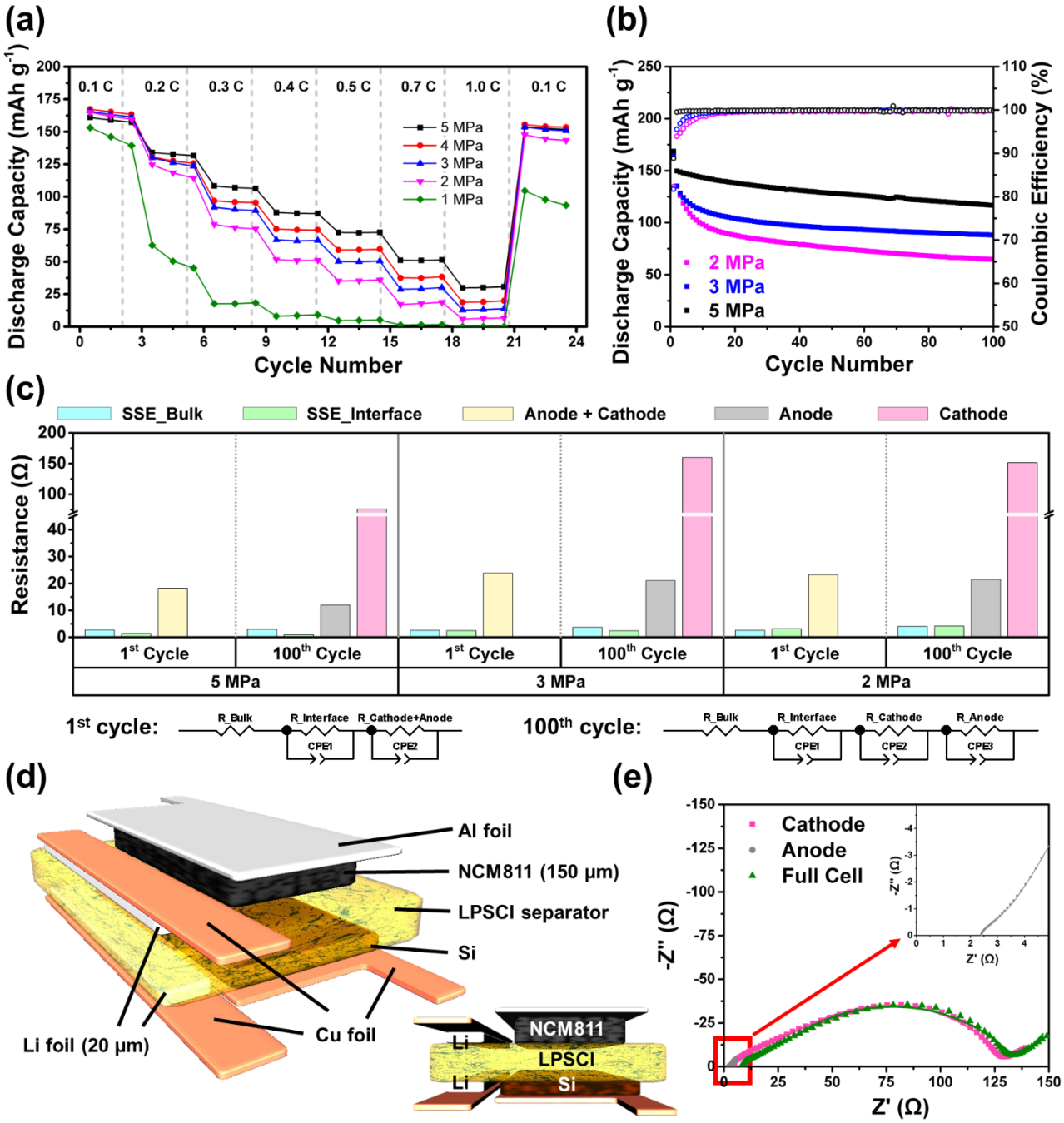

Figure 3. (a) Rate capability test of pouch cells with different cycling pressure at different current densities. (b) The capacity retention and Coulombic efficiency plots of pouch cells fabricated at 500 MPa and cycled at 5 MPa, 3 MPa and 2 MPa. (c) The EIS fitting results of the pouch cells measured after 1st and 100th cycle at 50% state of charge. (d) The schematic of the structure of a three-electrode ASSPC. (e) The Nyquist plots of cathode – Li, anode – Li and full cell (anode – cathode) EIS at 50% state of charge in 11th discharge.

For practical use, isostatic ASSPC modules may occasionally need to be depressurized during idling, and the effect of depressurizing on electrochemical performance needs to be evaluated. To probe the impedance evolution of ASSPCs under pressure change when it is not in operation, an ASSPC after 100 cycles was

subjected to a pressure decrease from 5 to 1 MPa. It was then re-pressurized back to 5 MPa and at last re-calendered at 500 MPa (the detailed procedure is described in **Chart S1**). The EIS results are presented in **Figure 4a**, **Figure S8** and **Table S2**. As the pressure decreased, the impedance of the cell gradually increased. While the impedance of the SSE separator layer increased by 1.7 times, both the interfacial impedance at the anode and the cathode increased approximately 2.5 times when the pressure decreased from 5 MPa to 1 MPa. The impedance of the ASSPC could not be restored even if the pressure resumed to 5 MPa. To restore the initial cell architecture, the ASSPC was re-calendered at 500 MPa and the impedance dropped significantly. Consequently, **Figure 4b** shows that the re-calendered ASSPC exhibited a higher discharge capacity of 141.2 mAh g^{-1} than that before it was re-calendered (116.5 mAh g^{-1}). To further validate the impact of re-calendering, the ASSPC that underwent the rate capability test at 1 MPa was subjected to re-calendering and then cycled again at 5 MPa. The performance was also almost fully restored, similar to the ASSPC cycled at 5 MPa from the beginning (**Figure 4c** and **Figure S9**). The impedance change suggests that there is a microstructure evolution in the cathode composite as a function of the applied pressure (**Figure 4d**). When the applied pressure decreases, both SSE and cathode particles can undergo volume relaxation to their low-pressure state. This creates larger gaps, resulting in poor interfacial contact, and thus increases the cell impedance. As the friction between particles needs to be mitigated to eliminate gaps, high calendering pressure is required to reform the physical contact. It is worthy to note that the impedance could not be fully restored, as SEI and cathode electrolyte interface (CEI) had formed after long cycling.[39]

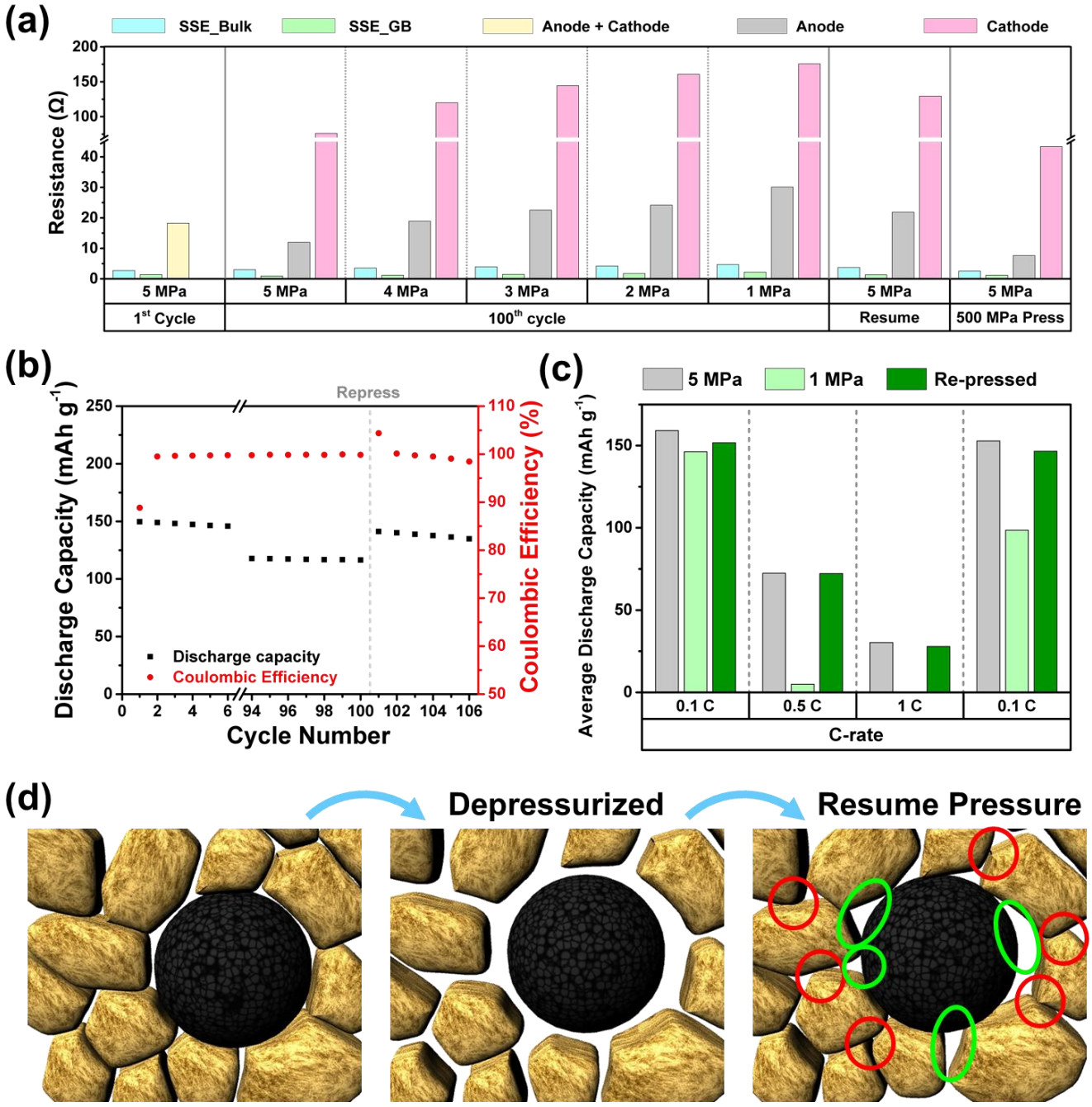

Figure 4. (a) The EIS results of the ASSPC cycled at 5 MPa after 100 cycles, after decreasing the pressure to 1 MPa, resuming at 5 MPa, and then re-calendered at 500 MPa. (b) the capacity retention and CE of the pouch cell cycled at 5 MPa before and after re-calendering. (c) The average discharge capacity of the pouch cell having rate test at 1 MPa, re-calendering at 500 MPa, and having another rate test at 5 MPa. (d) Schematic of the microstructure evolution between SSE and cathode when insufficient pressure is applied and the inability to restore to their original state even after the pressure returns to the initial value (red circles label the friction spots and green circles label the gaps). A much higher pressure must be applied to restore the contact between particles.

To validate the feasibility of a multi-layer pouch cell in IPCHs, a bilayer ASSPC (Cu | Si | SSE | NCM811

| Al | NCM811 | SSE | Si | Cu) with a total cathode area of 21 cm^2 and an areal theoretical capacity of approximately 5 mAh cm^{-2} (which led to a total theoretical capacity of over 100 mAh) was assembled, and cycled at 5 MPa, 30 °C and 0.1 C. The FIB-SEM cross-sectional images and the details of the cell format are shown in **Figure 5a**. The bilayer ASSPC exhibited an initial Coulombic efficiency of 76.9% and discharge capacity of 173.6 mAh g^{-1} (88.1 mAh) which is close to the single layer pouch cell, indicating they have similar material utilization. After 100 cycles, a discharge capacity of 145.0 mAh g^{-1} was retained (**Figure 5b-c**). To examine the power capability of the bilayer ASSPC, it was used to power an incandescent light bulb with a rating of 2.5 V and 300 mA (**Figure 5d**), highlighting its ability to be discharged at 3 C. Although the current IPCH design might look bulky, its energy density can be further boosted by accommodating multiple ASSPCs in its chamber and improved module design.

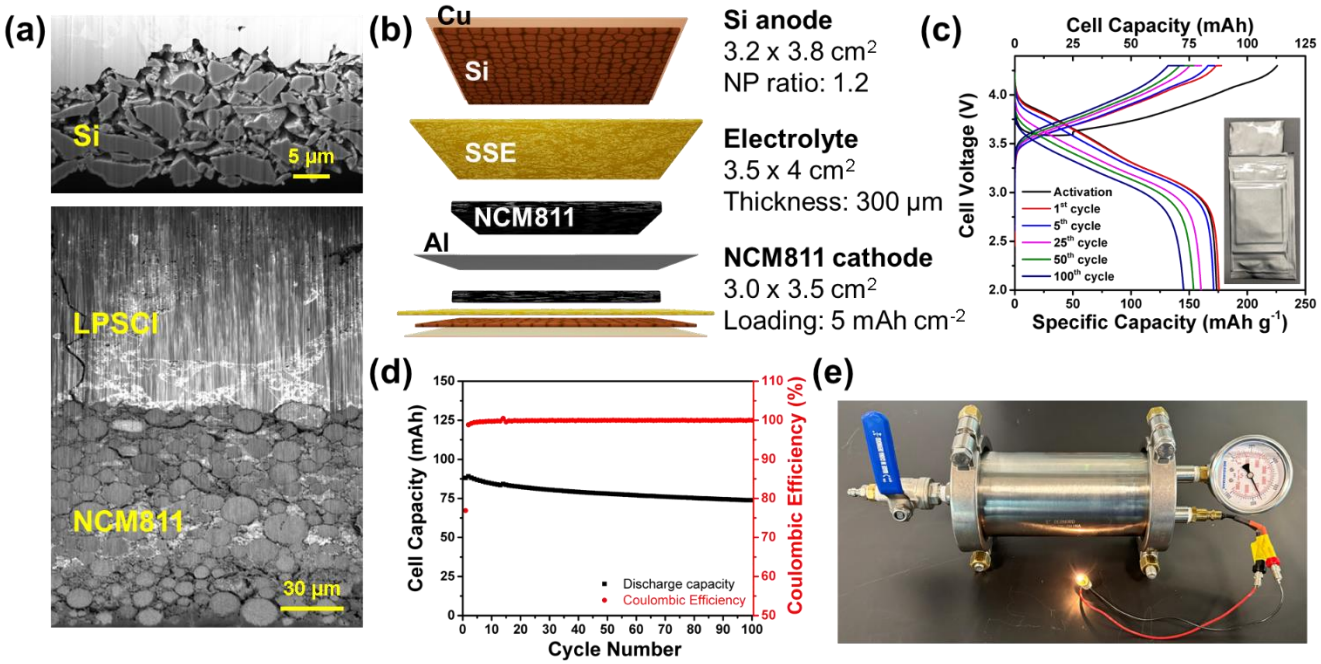

Figure 5. (a) The P-FIB SEM cross-section and (b) the schematic and illustrating the bilayer pouch cell configuration. The (c) voltage profiles at different cycle numbers and (d) capacity retention of the 3 × 3.5 cm^2 bilayer ASSPC. (e) A bilayer ASSPC powering an incandescent light bulb with an input rating of 2.5 V – 300 mA under5 MPa of isostatic cycling pressure.

Conclusion

As cycling pressure is required to maintain good interfacial contacts between different components in ASSBs, it is important to develop a pressurization system that enables uniform and accurate pressure to boost the electrochemical performance of ASSBs. In this study, we developed an IPCH that employed compressed air to apply a more homogenously distributed pressure than that of UPCHs with rigid metal surfaces or flexible rubber gaskets. As fluids do not suffer from material fatigue like many solid elastic materials, the IPCH enabled a higher capacity retention of an ASSPC than that of a UPCH over 100 cycles crediting to its stable

pressurization. The minimum required cycling pressure to cycle NCM811 | LPSCl | Si ASSPCs was found to be as low as 2 MPa to deliver acceptable electrochemical performances, even at 1 C. However, a higher pressure is still preferred to maintain the intimate contact during long-term cycling. Additionally, the NCM811 cathode composite was found to contribute the most to the overall cell impedance, and thus accentuated the importance of optimizing cathode composites for future research. A bilayer ASSPC cycled in an IPCH showed a practical capacity of approximately 88.1 mAh at 0.1 C for 50 cycles. Moreover, the cell was capable of discharging at a rate of 3 C (300 mA) powering an incandescent light bulb. The concept of isostatic pressurization in this study not only provides a uniform and accurate pressurizing method to study the pressure effects on ASSPCs, but also endeavors on the commercialization of ASSBs.

Experimental

1. Fabrication of electrolytes and SSE separators.

Dry-processed $LiNi_{0.8}Co_{0.1}Mn_{0.1}O_2$ (NCM811, LG Energy Solution) cathode composite, dry-processed Li_6PS_5Cl (LPSCl, NEI Corporation) SSE separator and slurry-processed Si anode were employed in ASSPCs. To fabricate NCM811 cathode composite, NCM811, LPSCl, vapor grown carbon fiber (VGCF, Sigma-Aldrich) and polytetrafluoroethylene (PTFE) were mixed in a mortar and a pestle at a weight ratio of 66 : 31 : 3 : 0.1 until a dough formed. The dough was then transferred to a hot roller (TMAXCN) set at 60 °C to fabricate films following the protocol described in the previous article.[40] Shear force was applied during mixing and rolling to fibrillate PTFE and strengthen the films.[40-43] A similar procedure was applied to fabricate LPSCl SSE separator, with a weight ratio of LPSCl : PTFE = 99.9 : 0.1. To prepare μ-Si electrodes, 99.9 wt.% μ-Si (Thermofisher) powder and 0.1 wt.% PVDF binder was dispersed in N-Methyl-2-Pyrrolidone (NMP) solvent using a Thinky mixer to create a slurry. The slurry was casted on a piece of 10 μm copper foil current collector using a doctor blade on an automatic film coater. The electrode was vacuum dried at 80 °C overnight to remove the solvent. The dried electrode was then punched into suitable shapes to be used for ASSPC fabrication.

2. Fabrication of ASSPCs.

Three pouch cell formats were used in this study: two-electrode, three-electrode electrochemical characterization cells, and bilayer cells. Cathode composite films with a dimension of 15 mm × 35 mm × 160 μm (resulting in an areal loading of 4 mAh cm^{-2}), SSE separators with a dimension of 20 mm × 50 mm × 300 μm, and Si anode with NP ratio of 1.2 and a dimension of 18 mm × 40 mm were selected for two-electrode electrochemical characterization cells. The area of the cathode composite films was the smallest, as it was selected as the capacity limiting component, and SSE separators were the largest to electronically separate cathodes and anodes. To assemble an electrochemical characterization cell, Cu, Si, LPSCl, NCM811 cathode composite and Al were stacked from bottom to top and secured with Kapton tape. An Al tab was welded to the Al current collector as the positive terminal, and a Ni tab to the Cu current collector as the negative terminal (both terminals are 4 mm in width). The whole stack was then vacuum sealed in the Al laminated film and calendered using a cold isostatic press (MTI Corporation). To understand the effect of calender pressure on the electrochemical performance, ASSPCs calendered at 150, 350 and 500 MPa with three-minute hold time were cycled and characterized **(Figure S10-11** and **Note S2**). 500 MPa was selected to calendar the ASSPCs to study

the effect of cycling pressure, as it was the largest pressure that the equipment could provide and yielded the best electrochemical performance. After calendering, cycling pressures were applied to ASSPCs using UPCHs and IPCHs. When torquing the bare UPCH, a torque wrench was used to torque all four nuts sequentially and the torque value was gradually increased in each rotation to the target value to ensure parallelism of the metal plates. A high-pressure air compressor was used to apply cycling pressure for IPCHs. To fabricate three-electrode electrochemical characterization cells, the horizontal dimensions of cathodes and anodes were reduced to 10 mm × 35 mm and 12 mm × 40 mm. Two pieces of Li metal (20 µm thick, Honjo Chemical Cooperation) were placed next to the cathode and anode, and on both sides of the SSE separator (**Figure S7a**). The cells were calendered at 150 MPa with a short hold time to prevent excessive Li-creeping. The rest of the fabrication steps were identical to those of two-electrode electrochemical characterization cells. Cathode composite films with a dimension of 30 mm × 35 mm × 200 µm (resulted in an areal loading of 5 mAh cm^{-2}), SSE separators with a thickness of 35 mm × 40 mm 300 µm, and Si anode with NP ratio of 1.2 and a dimension of 35 mm × 37 mm were selected for bilayer cells. They were stacked in a sequence of Cu, Si, LPSCl, NCM811 cathode composite, Al, NCM811 cathode composite, LPSCl, Si, and Cu. The rest of the fabrication steps were identical to those of electrochemical characterization cells.

3. Galvanostatic cycling and Electrochemical impedance spectroscopy (EIS) of ASSPCs

Neware A211-BTS-4S-1U-100mA-124 battery cyclers and a Biologic VSP-300 were employed for galvanostatic cycling and EIS measurements. A voltage cutoff of 2 to 4.3 V was selected for NCM811 | Si system.[6] As Li diffusivity in pure Si can be improved only after lithiation[6], an activation cycle was introduced in all testing protocols. In the activation cycle, ASSPCs were cycled at 0.05 C for 5 hours, and then completed the whole cycle at 0.1 C. A pressure of 5 MPa was applied in the activation cycle and later reduced to their target pressures. To obtain accurate cycling data, all ASSPCs were cycled in an oven set at 30 °C to study the effect of cycling pressure. The rate capability test was conducted by running the ASSPCs at 0.1, 0.2, 0.3, 0.4, 0.5, 0.7, 1 and 0.1 C and each C-rate for 3 cycles under 5 to 1 MPa. In the long-term cycling test, ASSPCs were cycled at 0.2 C and a constant voltage step till 0.05 C was applied at the end of charging. The ASSPCs were cycled for 100 cycles and EIS was obtained in the 1^{st} and 100^{th} cycle at 50% state of charge during discharge. Z-View software was used to analyze EIS results. The EIS of a three-electrode ASSPC was recorded at the ambient temperature in the 11^{th} cycle at state of charge of 50% during discharge. NCM811 cathode, Si anode and Li metal electrode were connected to working, counter and reference electrodes. Afterwards, the three-electrode ASSPC was cycled using Biologic VSP-300 at ambient temperature to record the voltage profiles of cathode – Li, anode – Li and full cell. The bilayer ASSPC was cycled at 0.1 C and a constant voltage step till 0.05 C was applied at the end of charging.

4. Characterization and image processing

A Helios G4 PFIB UXe DualBeam plasma focused ion beam / scanning electron microscope (P-FIB / SEM) with a xenon source was used to obtain the cross section of ASSPCs. After the ASSPCs were calendered, they were disassembled, and their cathode composites were attached to SEM stubs and sealed in an Ar-filled glovebox. The stubs were then transferred to P-FIB / SEM within 30 seconds of air exposure. Sample milling

was conducted at 30 kV with a 2.5 µA current. Afterwards, a lower current (500 and 60 nA) was used to polish the cross-section. Electron imaging was conducted at 5 kV and 4 nA beam conditions. To segment the P-FIB / SEM images, they were imported into the Trainable Weka Segmentation Fiji module[44] to identify NMC811, LPSCl and pores. The segmentation relies on machine-learning algorithms that are manually trained by the user with the input images. The phase ratios were then computed in MATLAB. The images of pressure paper were also processed: based on pictures of the pressure papers, the results were re-scaled in MATLAB using the ratio between the red color and the green and blue colors for each pixel in the jpg files.

Conflict of interest

Two joint patent applications on this work have been filed (US 63/546,685 and US 63/547,809) between UC San Diego's Office of Innovation and Commercialization as well as LG Energy Solution, Ltd.

Acknowledgement

This work was partially supported by LG Energy Solution through the Frontier Research Laboratory (FRL) program. Part of this work was performed at the San Diego Nanotechnology Infrastructure (SDNI) of the UCSD, a member of the National Nanotechnology Coordinated Infrastructure, supported by the National Science Foundation (Grant ECCS-1542148). The authors acknowledge the use of facilities and instrumentation at the UC Irvine Materials Research Institute (IMRI) supported in part by the National Science Foundation Materials Research Science and Engineering Center program through the UC Irvine Center for Complex and Active Materials (DMR-2011967). The authors also acknowledge the support from Coherent/II-VI Foundation.

References

1. Horowitz, Y.; Schmidt, C.; Yoon, D.-h.; Riegger, L. M.; Katzenmeier, L.; Bosch, G. M.; Noked, M.; Ein-Eli, Y.; Janek, J.; Zeier, W. G., Between Liquid and All Solid: A Prospect on Electrolyte Future in Lithium-Ion Batteries for Electric Vehicles. *Energy Technology* **2020,** *8* (11), 2000580.
2. Jung, Y. S.; Oh, D. Y.; Nam, Y. J.; Park, K. H., Issues and challenges for bulk-type all-solid-state rechargeable lithium batteries using sulfide solid electrolytes. *Isr. J. Chem.* **2015,** *55* (5), 472-485.
3. Kerman, K.; Luntz, A.; Viswanathan, V.; Chiang, Y.-M.; Chen, Z., practical challenges hindering the development of solid state Li ion batteries. *J. Electrochem. Soc.* **2017,** *164* (7), A1731.
4. Lee, H.; Oh, P.; Kim, J.; Cha, H.; Chae, S.; Lee, S.; Cho, J., Advances and Prospects of Sulfide All-Solid-State Lithium Batteries via One-to-One Comparison with Conventional Liquid Lithium Ion Batteries. *Adv. Mater.* **2019,** *31* (29), 1900376.
5. Cangaz, S.; Hippauf, F.; Reuter, F. S.; Doerfler, S.; Abendroth, T.; Althues, H.; Kaskel, S., Enabling High-Energy Solid-State Batteries with Stable Anode Interphase by the Use of Columnar Silicon Anodes. *Adv. Energy Mater.* **2020,** *10* (34), 2001320.
6. Tan, D. H.; Chen, Y.-T.; Yang, H.; Bao, W.; Sreenarayanan, B.; Doux, J.-M.; Li, W.; Lu, B.; Ham, S.-Y.; Sayahpour, B., Carbon-free high-loading silicon anodes enabled by sulfide solid electrolytes. *Science* **2021,** *373* (6562), 1494-1499.
7. Chan, C. K.; Peng, H.; Liu, G.; McIlwrath, K.; Zhang, X. F.; Huggins, R. A.; Cui, Y., High-performance lithium battery anodes using silicon nanowires. *Nat. Nanotechnol.* **2008,** *3* (1), 31-35.
8. Wu, H.; Chan, G.; Choi, J. W.; Ryu, I.; Yao, Y.; McDowell, M. T.; Lee, S. W.; Jackson, A.; Yang, Y.; Hu, L., Stable cycling of double-walled silicon nanotube battery anodes through solid–electrolyte interphase control. *Nat. Nanotechnol.* **2012,** *7* (5), 310-315.
9. Liu, N.; Lu, Z.; Zhao, J.; McDowell, M. T.; Lee, H.-W.; Zhao, W.; Cui, Y., A pomegranate-inspired nanoscale design for large-volume-change lithium battery anodes. *Nat. Nanotechnol.* **2014,** *9* (3), 187-192.
10. Cui, L.-F.; Ruffo, R.; Chan, C. K.; Peng, H.; Cui, Y., Crystalline-amorphous core− shell silicon nanowires for high capacity and high current battery electrodes. *Nano Lett.* **2009,** *9* (1), 491-495.
11. Su, X.; Wu, Q.; Li, J.; Xiao, X.; Lott, A.; Lu, W.; Sheldon, B. W.; Wu, J., Silicon-based nanomaterials for lithium-ion batteries: a review. *Adv. Energy Mater.* **2014,** *4* (1), 1300882.
12. Banerjee, A.; Wang, X.; Fang, C.; Wu, E. A.; Meng, Y. S., Interfaces and interphases in All-Solid-State batteries with inorganic solid electrolytes. *Chem. Rev.* **2020,** *120* (14), 6878-6933.
13. Koerver, R.; Aygün, I.; Leichtweiß, T.; Dietrich, C.; Zhang, W.; Binder, J. O.; Hartmann, P.; Zeier, W. G.; Janek, J. r., Capacity fade in solid-state batteries: interphase formation and chemomechanical processes in nickel-rich layered oxide cathodes and lithium thiophosphate solid electrolytes. *Chem. Mater.* **2017,** *29* (13), 5574-5582.
14. Shi, T.; Zhang, Y.-Q.; Tu, Q.; Wang, Y.; Scott, M.; Ceder, G., Characterization of mechanical degradation in an all-solid-state battery cathode. *J. Mater. Chem. A* **2020,** *8* (34), 17399-17404.
15. Chen, Y.-T.; Duquesnoy, M.; Tan, D. H.; Doux, J.-M.; Yang, H.; Deysher, G.; Ridley, P.; Franco, A. A.; Meng, Y. S.; Chen, Z., Fabrication of high-quality thin solid-state electrolyte films assisted by

machine learning. *ACS Energy Letters* **2021,** *6* (4), 1639-1648.
16. Tan, D. H.; Meng, Y. S.; Jang, J., Scaling up high-energy-density sulfidic solid-state batteries: A lab-to-pilot perspective. *Joule* **2022,** *6* (8), 1755-1769.
17. Liu, S.; Zhou, L.; Han, J.; Wen, K.; Guan, S.; Xue, C.; Zhang, Z.; Xu, B.; Lin, Y.; Shen, Y., Super Long-Cycling All-Solid-State Battery with Thin Li6PS5Cl-Based Electrolyte. *Adv. Energy Mater.* **2022,** *12* (25), 2200660.
18. Wang, C.; Kim, J. T.; Wang, C.; Sun, X., Progress and Prospects of Inorganic Solid-State Electrolyte-Based All-Solid-State Pouch Cells. *Adv. Mater.* **2023,** *35* (19), 2209074.
19. Dixit, M.; Beamer, C.; Amin, R.; Shipley, J.; Eklund, R.; Muralidharan, N.; Lindqvist, L.; Fritz, A.; Essehli, R.; Balasubramanian, M., The Role of Isostatic Pressing in Large-Scale Production of Solid-State Batteries. *ACS Energy Letters* **2022,** *7* (11), 3936-3946.
20. Lee, Y.-G.; Fujiki, S.; Jung, C.; Suzuki, N.; Yashiro, N.; Omoda, R.; Ko, D.-S.; Shiratsuchi, T.; Sugimoto, T.; Ryu, S., High-energy long-cycling all-solid-state lithium metal batteries enabled by silver–carbon composite anodes. *Nat. Energy* **2020,** *5* (4), 299-308.
21. Zhang, F.; Guo, Y.; Zhang, L.; Jia, P.; Liu, X.; Qiu, P.; Zhang, H.; Huang, J., A review of the effect of external pressure on all-solid-state batteries. *Etransportation* **2022**, 100220.
22. Koerver, R.; Zhang, W.; de Biasi, L.; Schweidler, S.; Kondrakov, A. O.; Kolling, S.; Brezesinski, T.; Hartmann, P.; Zeier, W. G.; Janek, J., Chemo-mechanical expansion of lithium electrode materials–on the route to mechanically optimized all-solid-state batteries. *Energy Environ. Sci.* **2018,** *11* (8), 2142-2158.
23. Ham, S.-Y.; Yang, H.; Nunez-cuacuas, O.; Tan, D. H.; Chen, Y.-T.; Deysher, G.; Cronk, A.; Ridley, P.; Doux, J.-M.; Wu, E. A., Assessing the critical current density of all-solid-state Li metal symmetric and full cells. *Energy Storage Materials* **2023,** *55*, 455-462.
24. Lin, D.; Liu, Y.; Cui, Y., Reviving the lithium metal anode for high-energy batteries. *Nat Nanotechnol* **2017,** *12* (3), 194-206.
25. Ito, S.; Fujiki, S.; Yamada, T.; Aihara, Y.; Park, Y.; Kim, T. Y.; Baek, S.-W.; Lee, J.-M.; Doo, S.; Machida, N., A rocking chair type all-solid-state lithium ion battery adopting Li2O–ZrO2 coated LiNi0. 8Co0. 15Al0. 05O2 and a sulfide based electrolyte. *J. Power Sources* **2014,** *248*, 943-950.
26. Sakuda, A.; Kuratani, K.; Yamamoto, M.; Takahashi, M.; Takeuchi, T.; Kobayashi, H., All-solid-state battery electrode sheets prepared by a slurry coating process. *J. Electrochem. Soc.* **2017,** *164* (12), A2474.
27. Nam, Y. J.; Oh, D. Y.; Jung, S. H.; Jung, Y. S., Toward practical all-solid-state lithium-ion batteries with high energy density and safety: comparative study for electrodes fabricated by dry-and slurry-mixing processes. *J. Power Sources* **2018,** *375*, 93-101.
28. Yuan, H.; Nan, H. X.; Zhao, C. Z.; Zhu, G. L.; Lu, Y.; Cheng, X. B.; Liu, Q. B.; He, C. X.; Huang, J. Q.; Zhang, Q., Slurry-coated sulfur/sulfide cathode with Li metal anode for all-solid-state lithium-sulfur pouch cells. *Batteries & Supercaps* **2020,** *3* (7), 596-603.
29. Fiedler, M.; Cangaz, S.; Hippauf, F.; Dörfler, S.; Abendroth, T.; Althues, H.; Kaskel, S., Mechanistic Insights into the Cycling Behavior of Sulfur Dry-Film Cathodes. *Advanced Sustainable*

Systems **2023**, 2200439.
30. Li, J.; Li, Y.; Zhang, S.; Liu, T.; Li, D.; Ci, L., Long cycle life all-solid-state batteries enabled by solvent-free approach for sulfide solid electrolyte and cathode films. *Chem. Eng. J.* **2023,** *455*, 140605.
31. Zhang, Z.; Chen, S.; Yang, J.; Wang, J.; Yao, L.; Yao, X.; Cui, P.; Xu, X., Interface re-engineering of Li10GeP2S12 electrolyte and lithium anode for all-solid-state lithium batteries with ultralong cycle life. *ACS applied materials & interfaces* **2018,** *10* (3), 2556-2565.
32. Hori, S.; Kanno, R.; Sun, X.; Song, S.; Hirayama, M.; Hauck, B.; Dippon, M.; Dierickx, S.; Ivers-Tiffée, E., Understanding the impedance spectra of all-solid-state lithium battery cells with sulfide superionic conductors. *J. Power Sources* **2023,** *556*, 232450.
33. Cao, D.; Sun, X.; Li, Y.; Anderson, A.; Lu, W.; Zhu, H., Long-Cycling Sulfide-Based All-Solid-State Batteries Enabled by Electrochemo-Mechanically Stable Electrodes. *Adv. Mater.* **2022,** *34* (24), 2200401.
34. An, S. J.; Li, J.; Daniel, C.; Kalnaus, S.; Wood, D. L., Design and demonstration of three-electrode pouch cells for lithium-ion batteries. *J. Electrochem. Soc.* **2017,** *164* (7), A1755.
35. Li, X.; Zhang, M.; Yuan, S.; Lu, C., Research progress of silicon/carbon anode materials for lithium-ion batteries: structure design and synthesis method. *ChemElectroChem* **2020,** *7* (21), 4289-4302.
36. Li, J.-Y.; Xu, Q.; Li, G.; Yin, Y.-X.; Wan, L.-J.; Guo, Y.-G., Research progress regarding Si-based anode materials towards practical application in high energy density Li-ion batteries. *Materials Chemistry Frontiers* **2017,** *1* (9), 1691-1708.
37. Liu, H.; Sun, Q.; Zhang, H.; Cheng, J.; Li, Y.; Zeng, Z.; Zhang, S.; Xu, X.; Ji, F.; Li, D., The application road of silicon-based anode in lithium-ion batteries: From liquid electrolyte to solid-state electrolyte. *Energy Storage Materials* **2022**.
38. Zuo, X.; Zhu, J.; Müller-Buschbaum, P.; Cheng, Y.-J., Silicon based lithium-ion battery anodes: A chronicle perspective review. *Nano Energy* **2017,** *31*, 113-143.
39. Tan, D. H.; Wu, E. A.; Nguyen, H.; Chen, Z.; Marple, M. A.; Doux, J.-M.; Wang, X.; Yang, H.; Banerjee, A.; Meng, Y. S., Elucidating Reversible Electrochemical Redox of Li6PS5Cl Solid Electrolyte. *ACS Energy Letters* **2019,** *4* (10), 2418-2427.
40. Lee, D. J.; Jang, J.; Lee, J. P.; Wu, J.; Chen, Y. T.; Holoubek, J.; Yu, K.; Ham, S. Y.; Jeon, Y.; Kim, T. H., Physio-Electrochemically Durable Dry-Processed Solid-State Electrolyte Films for All-Solid-State Batteries. *Adv. Funct. Mater.* **2023**, 2301341.
41. Wang, C.; Yu, R.; Duan, H.; Lu, Q.; Li, Q.; Adair, K. R.; Bao, D.; Liu, Y.; Yang, R.; Wang, J., Solvent-free approach for interweaving freestanding and ultrathin inorganic solid electrolyte membranes. *ACS Energy Letters* **2021,** *7* (1), 410-416.
42. Li, Y.; Wu, Y.; Wang, Z.; Xu, J.; Ma, T.; Chen, L.; Li, H.; Wu, F., Progress in solvent-free dry-film technology for batteries and supercapacitors. *Mater. Today* **2022,** *55*, 92-109.
43. Hippauf, F.; Schumm, B.; Doerfler, S.; Althues, H.; Fujiki, S.; Shiratsuchi, T.; Tsujimura, T.; Aihara, Y.; Kaskel, S., Overcoming binder limitations of sheet-type solid-state cathodes using a solvent-free dry-film approach. *Energy Storage Materials* **2019,** *21*, 390-398.

44. Arganda-Carreras, I.; Kaynig, V.; Rueden, C.; Eliceiri, K. W.; Schindelin, J.; Cardona, A.; Sebastian Seung, H., Trainable Weka Segmentation: a machine learning tool for microscopy pixel classification. *Bioinformatics* **2017,** *33* (15), 2424-2426.